

# 7

## Interpretation of data from axial tests on saturated clays

### 7.1 One Real Axial-test Apparatus

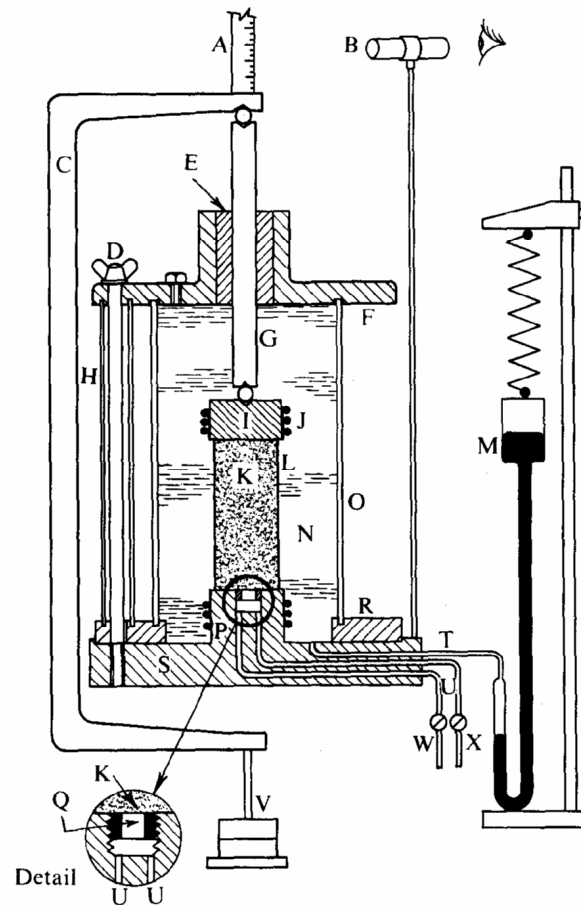
In conventional *strain-controlled* tests the loading ram of the axial-test cell is driven down at a constant rate: we will distinguish between the more usual *slow* tests in which the strain rates are chosen to achieve negligible pore-pressure gradients by the time of *ultimate* failure, and the rarer *very slow* tests in which the strain rates are chosen to achieve negligible pore-pressure gradients at *all stages* of yielding. The slow tests give ultimate data which we can interpret in terms of the critical state model for engineering design purposes: the very slow tests give data of yielding *before* the ultimate states which we can interpret by the Cam-clay model, and although this interpretation is too refined for use in practical engineering at present we consider that some understanding is helpful for correct use of the critical state model.

The Cam-clay model is based on a conceptual axial-test system that we introduced in chapter 5. We will now describe briefly a *stress-controlled* test apparatus that closely resembles the conceptual system. We do not regard this apparatus as ideal, but it does provide the standard of comparison by which we can judge whether published data of strain-controlled tests are or are not fully satisfactory for our particular purpose.

The original text<sup>1</sup> *The Measurement of Soil Properties in the Triaxial Test* by Bishop and Henkel of Imperial College, University of London, contains a detailed exposition of axial testing on the basis of extensive work by them and their students. A variation<sup>2</sup> of this original equipment by research workers at the Norwegian Geotechnical Institute with some slight modifications<sup>3</sup> introduced at Cambridge is illustrated in Fig. 7.1. We will describe one class of test only, the stress-controlled test; since our aim is not to present a general review of the many varieties of axial-test apparatus but to introduce a new approach to the analysis of the data, we will merely describe one test technique in sufficient detail to draw attention to the problems that must be overcome.

In Fig. 7.1 is shown a cylindrical specimen K of soil 4 in. long, 2 in. diameter standing on a 2¼ in. diameter pedestal P and supporting a loading cap I of the same diameter. A natural rubber latex membrane L of 0.01 in. thickness and 2 in. diameter when unstretched, envelopes the specimen and is closely bound to the loading cap and to the pedestal by highly stretched rubber O-rings J of 1½ in. internal diameter and ⅜ in. (unstretched) cross-sectional diameter. A mirror polish on the vertical surfaces of the pedestal and the loading cap minimizes the possibility of leakage of cell water past the bindings and into the pore-water.

The cell consists of a transparent plexiglass cylinder O permanently clamped between a top-plate F and a middle plate R by three lengths of threaded tube H. The cell is bolted down to the bottom-plate S by three long bolts with wing-nuts D. When the cell is assembled, the loading ram G that passes through a bushing E in the centre of the top plate is accurately co-axial with the pedestal P that is in the centre of the bottom plate. The bushing E is rotated at a constant rate by a small auxiliary motor, so there is effectively no friction resisting vertical movement of the ram through the bushing.



Not to scale

Fig. 7.1 Stress-controlled Axial-test Apparatus

The cell-water N fills the cell and surrounds the sheath, loading cap, and pedestal. A thin tube T connects the cell-water to a constant pressure device M of a type devised by Bishop and described by him (*loc. cit.*) as the self-compensating mercury control. This consists of a pot of mercury suspended by a spring, with leakage of water out of the cell causing the mercury to flow from the hanging pot; the consequent reduction in weight of the pot causes a shortening of the spring length which is so designed to maintain the mercury level constant and exactly sustain a constant pressure in the cell-water.

The bottom of the loading cap has a mirror polish and is lightly greased. The top of the pedestal also has a mirror polish and is lightly greased, except in the centre where a  $\frac{1}{4}$  in. diameter porous stone Q allows drainage of pore-water from the specimen. Thus the ends of the specimen are effectively free to expand laterally<sup>4</sup> by about 12 per cent. The porous stone is itself mounted in a short length of threaded tube (see detail in Fig. 7.1) which is screwed down into a small recess in the top of the pedestal. From the recess two lengths of  $\frac{1}{16}$  in. diameter 'hypodermic' steel tube U connected the pore-water with two devices outside the cell.

One device W is a back-pressured burette shown in Fig. 7.2(a). This burette Y is enclosed in a cylinder in which a constant water pressure is maintained by a second self-compensating mercury control. Changes in the silicone oil levels in the top of the cylinder and the burette show clearly the volume of pore-water that drains out of the specimen. The second device X is an accurate pore-pressure transducer which measures the change of pore-pressure that occurs when drainage is prevented. In Fig. 7.2(b) we show the system that was introduced by Bishop and has been widely used. Change of pore-pressure tends to

alter the level of the mercury  $Z$  in the 1 mm bore glass tube: this tendency is observed and counteracted by adjustment of the control cylinder so that the mercury level and hence the volume of pore-water within the specimen are kept constant. The pore-pressure  $u_w$  is indicated directly on the Bourdon gauge.

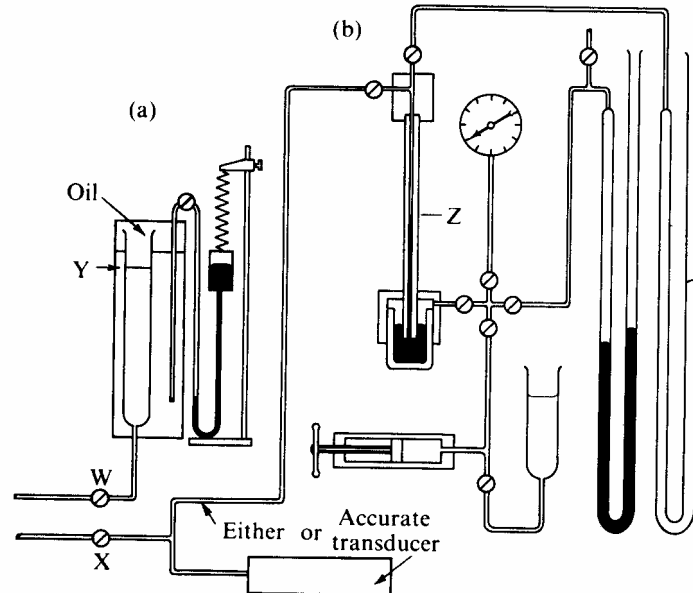


Fig. 7.2 Devices for Measuring Volume and Pressure of Pore-water

The loading ram  $G$  tends to be blown out of the bushing by the cell pressure; it is held down by a hanger  $C$  carrying a load  $V$ . A measuring telescope  $B$  fixed to a vertical bar that rises above the cell from the base is focussed on to a vertical scale  $A$  fixed to the hanger, so that change of the axial length of the specimen can be observed directly.

This particular apparatus permits study of specimens in a stress-controlled manner similar to that outlined in §5.2, etc. Each successive load-increment can be left long enough for the specimen to attain 100 per cent primary consolidation, and to be considered to be in equilibrium, because we have assumed that secondary phenomena are to be neglected.

The small but significant secondary displacements that occur over long periods after primary consolidation form a difficult topic of current research interest. We are faced with a rate process that is something other than Terzaghi's primary diffusion of water out of soil: it does appear that the best axial tests at a constant very slow strain rate give data that are more useful in this research than the standard stress-controlled test that we are describing.

## 7.2 Test Procedure

Two alternative test procedures commonly adopted are those for (a) the undrained test with pore-pressure measurement, and (b) the drained test. Both have much in common; the following brief account outlines the main features of what is a complicated technique and is only supposed to be a typical (but not perfect) test procedure. Readers of Bishop and Henkel (*loc. cit.*) will find much more on this point.

The first requirement is to ensure that the measuring devices  $W$  and  $X$  are free of air. The porous stone  $Q$  is removed from the base  $P$ , placed in a small evaporating dish and boiled. A temporary plug is screwed in its place and the pore-water system is checked by

forcing de-aired water from the hand-operated ram of the apparatus X without detectable changes of the pore-water levels Y and Z.

When this check is complete the back-pressured burette is then set to a desired level, and the connecting tube W is closed. A thin film of silicone grease is smeared over the base P, the plug is removed, the recess is flooded with water, and the saturated porous stone is screwed into the recess without trapping any air. A small quantity of water is forced up through the stone to ensure saturation and then the connecting tube X to the pore-pressure measuring apparatus is closed. Any excess water is removed from the surface of the porous stone, and if possible the base is then placed in a humid compartment.

The soil specimen is trimmed in the humid compartment and placed centrally on the pedestal. The rubber membrane, which has been soaked in water, is expanded by external suction back against a tube of 2½ in. internal diameter and placed round the specimen. The greased loading cap is carefully placed on the specimen, and firmly held against vertical movement by a clamp. The rubber membrane is released from the expander so that it embraces the specimen, cap, and pedestal. Any air bubbles trapped between the specimen and membrane are worked out, and three bindings rings are then placed at each end. The specimen and base are removed from the humid compartment, and the specimen's length and diameter are accurately measured.

The cell is then placed round the specimen, filled with de-aired water and a little oil is introduced below the loading ram. A pressure of 100 lb/in.<sup>2</sup>, say, is applied simultaneously both to the cell-water and back-pressured burette and the valve W opened; if there is any air in the pore-water system it is detected by observing movement of the level Y in the burette.

The specimen can now be consolidated, if necessary, to some predetermined condition by reducing the back pressure on the burette to some value  $u_w$ . The specimen is then experiencing an effective spherical pressure  $\sigma'_l = \sigma'_r = (100 - u_w)$  and as consolidation takes place pore-water will drain into the burette. For some specimens the back pressure may need to be raised again to allow the specimen to swell to an over-compressed state.

The specimen having experienced the required consolidation history is ready for shearing. If the specimen is to undergo an undrained test the connection to the burette W is closed and that to the pore-pressure device X opened, whereas for a drained test the connection to the burette is left open. Successive increments of load are applied to the hanger and after each increment sufficient time is allowed for primary consolidation to occur. Observations are made of the axial load, the consequent axial displacement of the loading cap, and either of (a) the pore-pressure, or of (b) the level of pore-water in the back-pressured burette.

The succession of load-increments concludes (after failure) with removal of loads from the hanger. The back pressure is raised to equal the cell pressure and, after sufficient time for swelling, the level in the burette is observed. The back pressure and cell pressure are then reduced to that of the atmosphere and again the level in the burette is observed. The apparatus is dismantled and finally, in the humid compartment, the sheath is removed and the specimen removed for determination of its final weight and water content.

### 7.3 Data Processing and Presentation

The data of an axial test fall into three main categories:

(a) the measurements of specimen length, diameter, weight, etc., and readings of any

consolidation which must be applied to the specimen to bring it to the desired initial condition ( $p_0, v_0, q_0$ );

(b) test constants such as calibration of proving ring (or load transducer), thickness and strength of membrane, specific gravity of specimen, etc.; and

(c) readings of time, axial load, axial displacement, change of volume and/or pressure of pore-water, and change of cell pressure, which occur during the test proper.

From this information we want to evaluate a variety of parameters, such as  $p, v, q, \sigma'_l/\sigma'_r, \varepsilon$ , etc., and repetitive calculations such as these are ideally performed by electronic digital computers. A suitable computer program can readily be devised to meet the special requirements of a particular laboratory or investigation, and will depend on what computer is available so we shall not attempt to set out a 'standard' program.

Typical input and output data from such a program are included in appendix B (see page 209). These are for a very slow *strain-controlled* undrained axial compression test on a specimen of virgin compressed kaolin which forms one of a recent series of tests.<sup>5</sup> The particular choice of parameters was:

(a) Axial strain  $\sum \dot{\varepsilon}_l = \sum (-\delta/l)$

(b) Volumetric strain  $\sum (\dot{v}/v) = \sum (-\delta V/V)$

(c) Cumulative shear strain  $\sum \dot{\varepsilon} = \sum \dot{\varepsilon}_l - \frac{1}{3} \sum \dot{v}/v$

(d) Voids ratio  $e = v - 1$

(e) Pore-pressure  $u_w$

(f) Axial-deviator stress  $q$

(g) Mean normal stress  $p$

(h) Stress ratio  $\eta = q/p$

(i)  $q/p_e$  where  $p_e$  is Hvorslev's equivalent pressure

(j)  $p/p_e$

(k)  $v_\lambda$

(l)  $v_\kappa$

(m)  $\dot{v}_\kappa/v\dot{\varepsilon}$

(n)  $\dot{q}/p_e\dot{\varepsilon}$

(o)  $\dot{p}/p_e\dot{\varepsilon}$

(p)  $\dot{v}^p/v\dot{\varepsilon}$

#### 7.4 Interpretation of Data on the Plots of $v$ versus $\ln p$

One assumption of the Cam-clay model is that recoverable compression and swelling should be governed by one constant  $\kappa$  and take the form given by eq. (6.3)

$$v = v_0 - \kappa \ln(p/p_0).$$

Data of swelling and recompression of remoulded London clay specimens from Henkel<sup>6</sup> are shown in Fig. 7.3. (The technique of remoulding used in these tests involved severe handling of specimens at relatively low water-content. The general character of these data differs from that of data from tests where specimens are consolidated from a slurry in that different values of  $\Gamma$  are indicated.) Some hysteresis occurs but the curves can be approximated by eq. (6.3) taking as numerical value for London clay  $\kappa = 0.062 \pm 0.016$ .

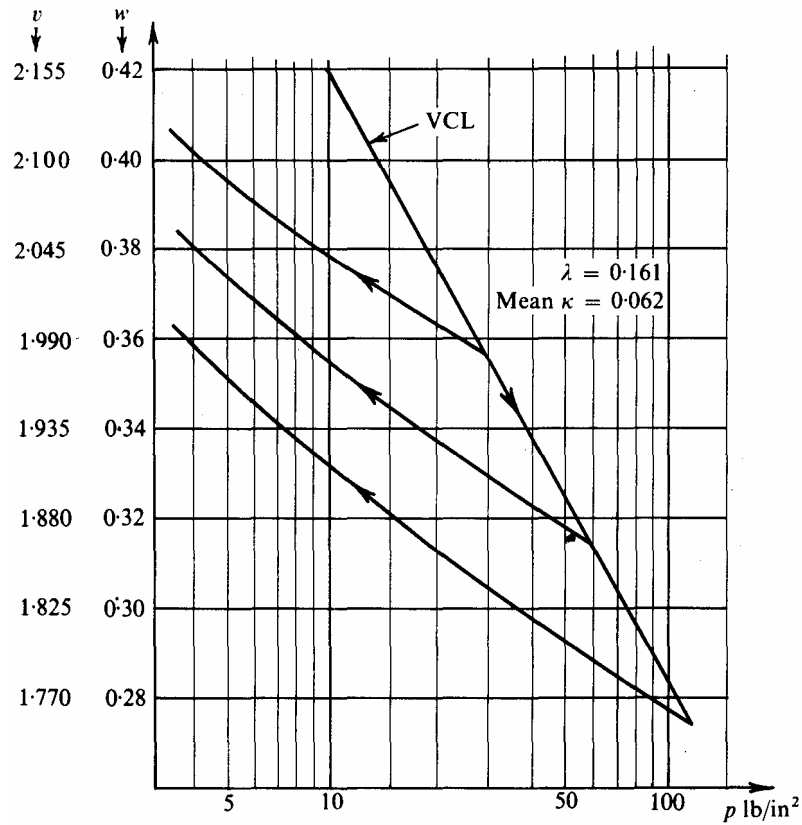


Fig. 7.3 Isotropic Consolidation and Swelling Curves for London Clay (After Henkel)

Having found values of  $\kappa$  and  $\lambda$  that are appropriate to the set of soil specimens under consideration we can compute  $v_\kappa$  and  $v_\lambda$ . We then know the coordinates of any point S in Fig. 7.4 either by values of  $v$  and  $p$ , or values of  $v_\kappa$  and  $v_\lambda$  which fix the  $\kappa$ -line and  $\lambda$ -line passing through the point S. We will be interested in changes of state of the specimen and can think of the current *state point* such as S and of a *state path* followed by a specimen during test.

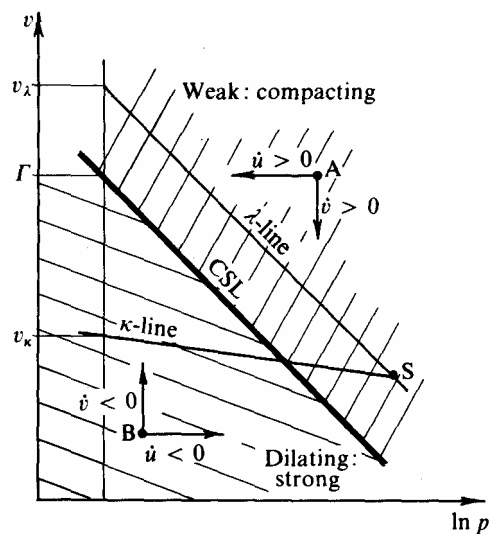


Fig. 7.4 Critical State Line Separating Differences in Behaviour of Specimens

One prediction shared by the Granta-gravel and Cam-clay models — see §5.9 — is that on the plot of  $v$  versus  $\ln p$  (Fig. 7.4) there should be a clear division between an area

of the plot in which specimens are weak at yield and either develop positive pore-pressures or compact, and another area in which specimens are strong at yield and either develop negative pore-pressures or dilate. These areas lie either side of a critical state curve, which should be one of the  $\lambda$ -lines for which  $v_\lambda = \Gamma$ .

Data of slow strain-controlled tests by Parry<sup>7</sup> on remoulded London clay specimens are shown in Fig. 7.5. For each specimen a moment of 'failure' occurs in the test when the system has become unstable and although the specimen is not wholly in a critical state, as will be discussed further in chapter 8, it is seen to be tending to come into the critical state. In Fig. 7.5(a) the data are points representing the following classes of specimens:

- (a) drained but showing zero rate of volume change at failure,
- (b) drained and showing continuing volume decrease at failure,
- (c) undrained but showing zero rate of pore-pressure change at failure,
- (d) undrained and showing continuing pore-pressure increase at failure.

All these points in Fig. 7.5(a) lie on the *wet* side of a certain straight A-line on the  $v$  versus  $\ln p$  plot. In contrast, in Fig. 7.5(b) the data are points representing the following classes of specimens:

- (a) drained and showing continuing volume increase at failure,
- (b) undrained and showing continuing pore-pressure decrease at failure.

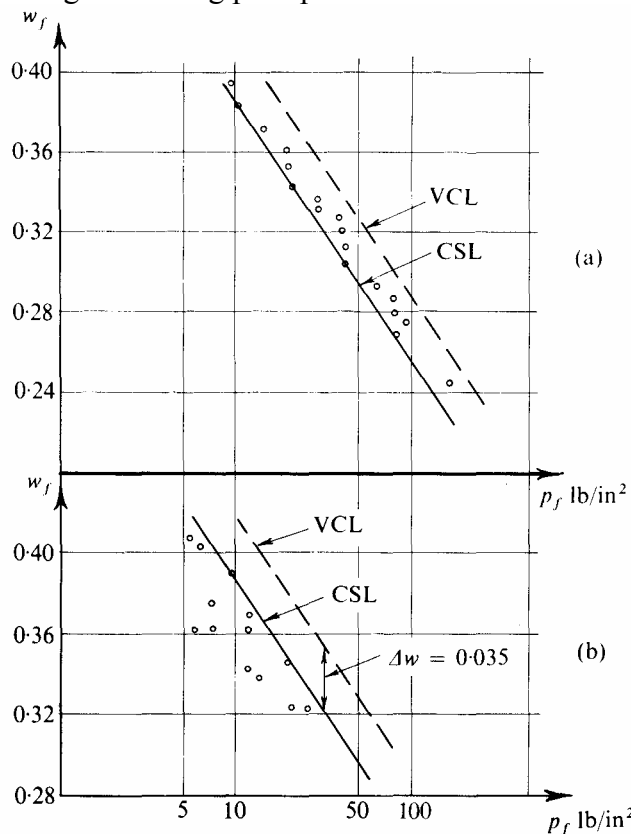


Fig. 7.5 Data of Tests on Remoulded London Clay at failure (After Parry)

All these points in Fig. 7.5(b) lie on the *dry* side of a certain  $\lambda$ -line on the  $v$  versus  $\ln p$  plot. We see that we have the *same*  $\lambda$ -line in Fig. 7.5(a) and (b). It closely resembles the predicted critical state line of Fig. 7.4.

A prediction of the Cam-clay model (§6.6) is that during compression under effective spherical pressure  $p$  the virgin compression curve is, from eq. (6.20) when  $\eta \rightarrow 0$ ,

$$v_\lambda = v + \lambda \ln p = \Gamma + (\lambda - \kappa) \quad (7.1)$$

so that it is displaced an amount  $\Delta v = (\lambda - \kappa)$  to the wet side of the critical state curve. In Fig. 7.5 the position of the virgin compression curve is indicated by Parry. It is displaced an amount  $\Delta v = G_s \Delta w \cong 2.75 \times 0.035 = 0.096$  to the wet side of the critical state curve: this is comparable with the prediction  $(\lambda - \kappa) = 0.099$ .

## 7.5 Applied Loading Planes

Having looked at the changing states of specimens on the  $v$  versus  $\ln p$  graph we now need to move away from the plane of  $v$  and  $p$  into the projections of  $(p, v, q)$  space in which we can see  $q$ . It is possible to relate geometrically the method of loading that we apply to the specimen, with the plane in which the state path of the test must lie, regardless of the material properties of the specimen.

In §5.5 it was shown that a specimen in equilibrium under some effective stress  $(p, q)$  will shift to a state  $(p + \dot{p}, q + \dot{q})$  when subject to a stress-increment. If the stress-increment is simply  $\dot{\sigma}_r = 0, \dot{\sigma}_l > 0$ , and if there is no pore-pressure change  $\dot{u}_w = 0$ , as in a drained test, then

$$\dot{p} = \frac{1}{3} \dot{\sigma}_l, \quad \dot{q} = \dot{\sigma}_l \quad (7.2)$$

giving the vector AB indicated in Fig. 5.7. We can thus introduce the idea of an applied loading plane in Fig. 7.6. Consider first in Fig. 7.6(a) the case of a drained compression test in which initially  $\sigma_l = p_0 = \sigma_r$  and then later  $\sigma_l > p_0$ . From eq. (7.2)  $dq/dp = 3$  and with initial conditions  $q = 0, p = p_0$ , we find

$$p = p_0 + \frac{1}{3}q, \quad (7.3)$$

which is the equation of the inclined plane of Fig. 7.6(a). The imposed conditions in the drained compression test are such that the state point  $(p, v, q)$  must lie in this plane.

Next consider the conditions imposed in §6.6, where we considered a drained yielding process with

$$\frac{\dot{q}}{\dot{p}} = \frac{q}{p} = \text{constant} = \eta > 0. \quad (6.21 \text{ bis})$$

In this case the principal effective stresses remain in constant ratio  $\sigma'_r/\sigma'_l = K$  where

$$K = \frac{3 - \eta}{3 + 2\eta}.$$

The imposed conditions in such a test require the state point to lie in the plane illustrated in Fig. 7.6(b).

The conditions imposed in the undrained test are such that  $\dot{v} = 0$ , and for this specimen the state points must lie in the plane  $v = v_0$  illustrated in Fig. 7.6(c).

Alternatively, it is possible to conduct extension tests in the axial-test apparatus for which  $\sigma_r > \sigma_l$  and  $q < 0$ . For a drained test of this type we have (from §5.5 and Fig. 5.7)

$$\frac{\dot{q}}{\dot{p}} = \frac{dp}{dq} = -\frac{2}{3}$$

and the applied loading plane becomes

$$p = p_0 - \frac{2}{3}q. \quad (7.4)$$

This is illustrated in Fig. 7.7; other examples could be found from tests in which the specimen is tested under conditions of constant  $p$ , or of constant  $q$  (as the mean normal



pressure is reduced), etc. At this stage we must emphasize that the applied loading planes are an indication only of the loading conditions applied by the external agency, and they are totally independent of the material properties of the soil in question.

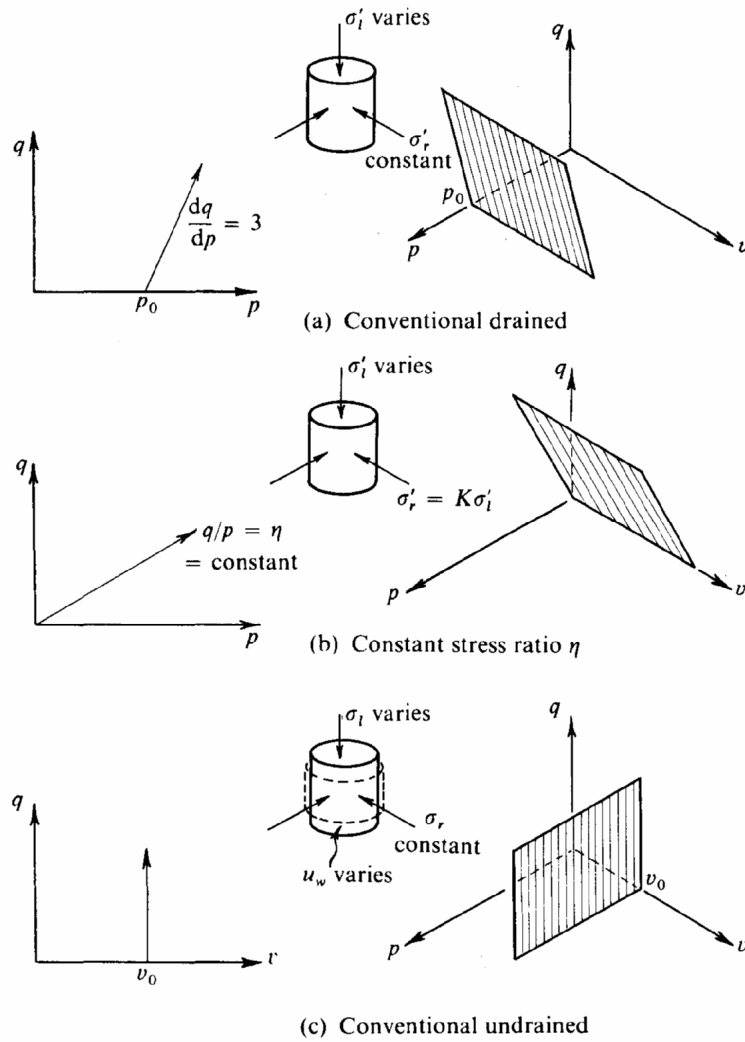


Fig. 7.6 Applied Loading Planes for Axial Compression Tests

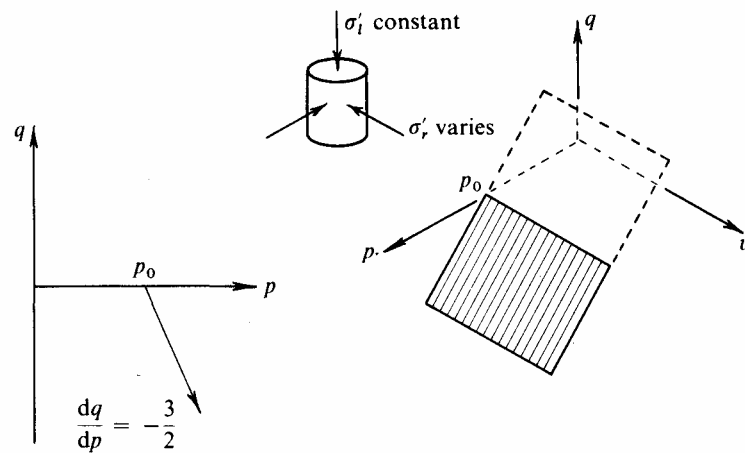


Fig. 7.7 Applied Loading Plane for Drained Axial Extension Test

## 7.6 Interpretation of Test Data in $(p, v, q)$ Space

The material properties of Cam-clay are defined in the surface shown in Fig. 6.5. If we impose on a specimen the test conditions of the *drained* compression test, the actual state path followed by the specimen must lie in the intersection of a plane such as that of Fig. 7.6(a) and the surface of Fig. 6.5. This intersection is illustrated in Fig. 7.8.

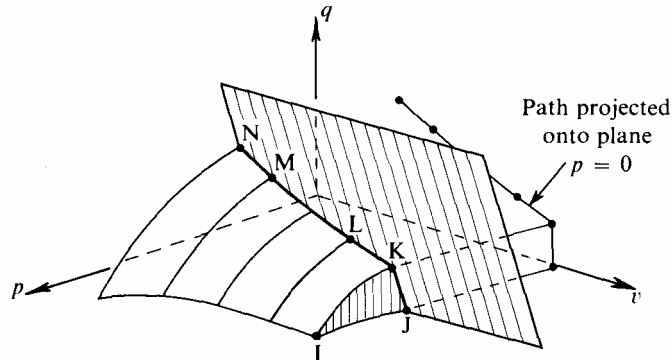


Fig. 7.8 State Path for Drained Axial Compression Test

The prediction of the Cam-clay model is fully projected in Fig. 7.9. We are considering a specimen virgin compressed to a pressure represented by point I and then allowed to swell back to a lightly overcompressed state represented by point J. The test path in Fig. 7.9(a) is the line JKLMN. The portion JK represents reversible behaviour before first yield at K; and in Fig. 7.9(b) this portion JK is seen to follow a re-compression curve (or  $\kappa$ -line). At K the material yields and hardens as it passes through states on successive (lightly drawn) yield curves. Simple projection locates points L, M, and N which then permit plotting of Fig. 7.9(c), which predicts the equilibrium values of the specific volume of a specimen under successive values of  $q$ .

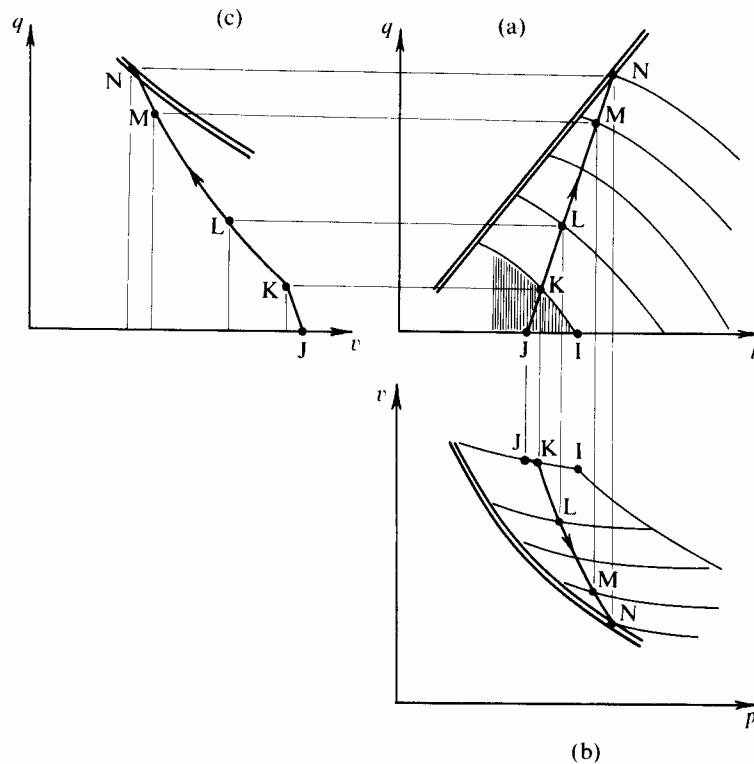


Fig. 7.9 Projections of State Path for Drained Axial Compression Test

In a similar manner, we appreciate in Fig. 7.10 that the intersection of the loading plane for an *undrained* compression test with the stable-state boundary surface must give the state path JFGH experienced by a similar specimen, which is shown projected in Fig. 7.11. Figure 7.11(a) and (b) show the plane  $v = v_0 = \text{const.}$  crossing various yield curves at F, G, H, and by simple projection we can plot the predicted stress path in Fig. 7.11(c).

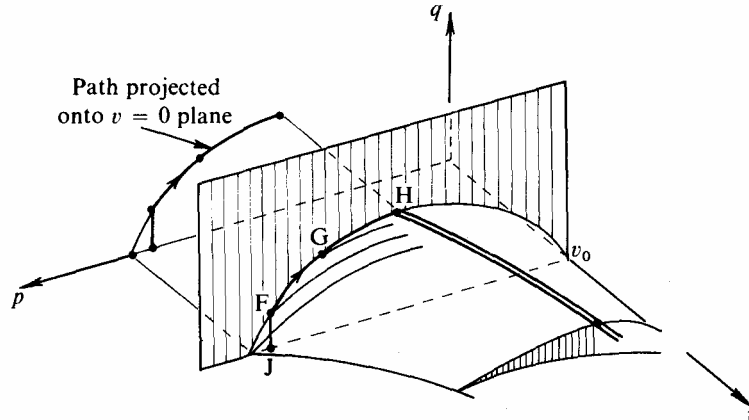


Fig. 7.10 State Path for Undrained Axial Compression Test

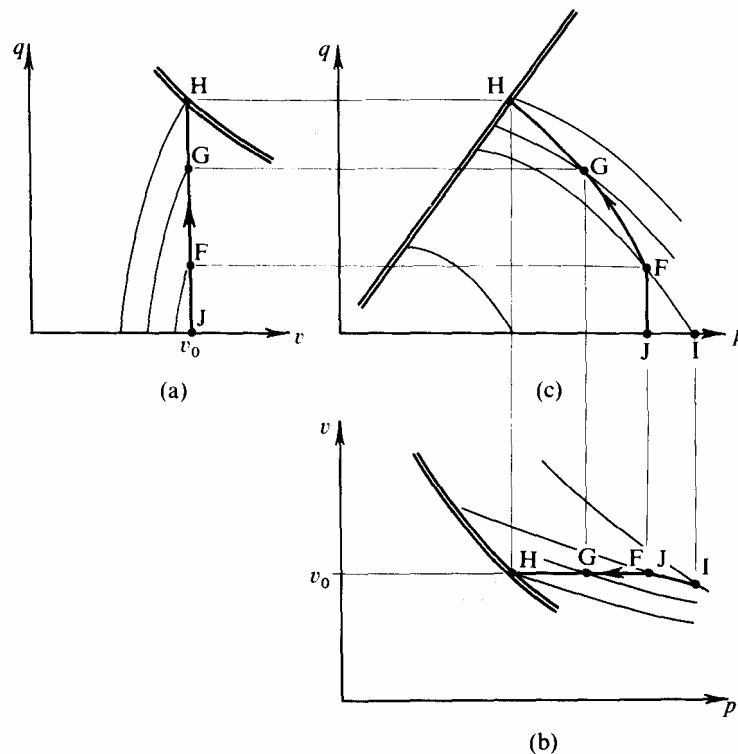


Fig. 7.11 Projections of State Path for Undrained Axial Compression Test

Data of a very slow strain-controlled undrained axial test are shown in Fig. 7.12: the specimen\* of London clay was initially in a state of virgin compression at the point E. The experimental points have been taken from results quoted by Bishop, Webb, and Lewin<sup>8</sup> (Test No. 1 of Fig. 17 of their paper) and replotted in terms of the stress parameters  $p$  and  $q$ . A prediction for this curve can be obtained from eq. (6.27)

\* In this case the specimen was prepared as a slurry at high water content and then consolidated, rather than being remoulded at relatively low water content. However, the form of this curve is similar to that found for remoulded specimens subject to the same test.

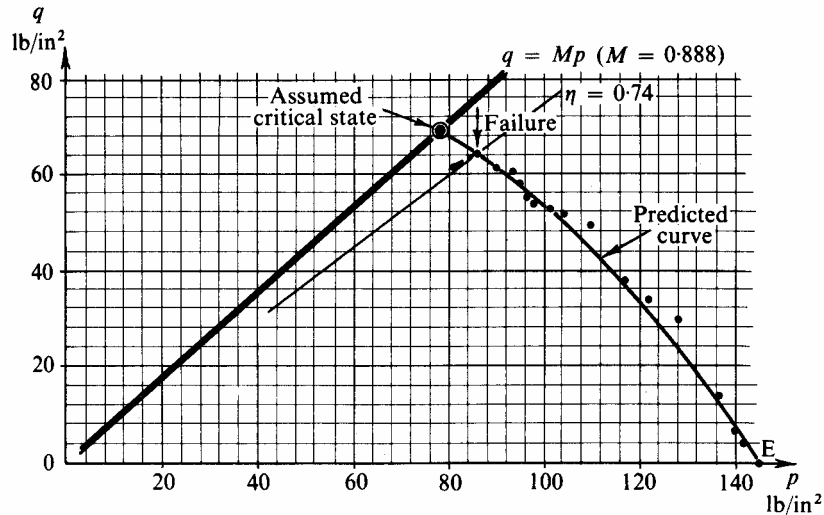


Fig. 7.12 Test Path for Undrained Axial Compression Test on Virgin Compressed Specimen of London Clay (After Bishop *et al.*)

$$|q| = \frac{Mp}{A} \ln\left(\frac{p_0}{p}\right) \quad (6.27 \text{ bis})$$

which was discussed in §6.7 and sketched in Fig. 6.7. Accepting previously quoted values of  $\lambda = 0.161$  and  $\kappa = 0.062$  for London clay, we find that with  $p_0 = 145 \text{ lb/in}^2$  and a choice of  $M = 0.888$  we can then predict an undrained test path which fits closely the observed test data. It is to be noted that the test terminates with a failure condition (defined by maximum  $q$ ) before an ultimate critical state is reached: we will have more to say about ‘failure’ in chapter 8.

## 7.7 Interpretation of Shear Strain Data

From the Cam-clay model we can predict the cumulative (permanent) distortional strain  $\varepsilon$  experienced by a specimen. Examples where calculations can be made in a closed form are for *undrained* tests and *p*-constant tests which have already been discussed briefly in §6.7 and §5.13 respectively. The discussion in §5.13 is strictly limited to Granta-gravel, but exactly similar development for Cam-clay leads to similar results for constant-*p* tests, i.e.,

$$M\varepsilon = \frac{\lambda - \kappa}{v_0 - D_0} \ln\left\{ \frac{D_0 v}{v_0(v - v_0 + D_0)} \right\}$$

which reduces to eq. (5.36) when  $\kappa = 0$ .

If we consider the case of the test on a virgin compressed specimen of London clay (prepared from a slurry) of Fig. 7.12, the relevant equations for an undrained test are:

$$\left. \begin{aligned} |q| &= \frac{Mp}{A} \ln(p_0/p) & (6.27 \text{ bis}) \\ \ln(p_0/p) + A &= \ln(p/p_u) = A \exp\left(\frac{-Mv_0}{\kappa A} \varepsilon\right) & (6.30 \text{ bis}) \\ \frac{|q|}{Mp} &= 1 - \exp\left(\frac{-Mv_0}{\kappa A} \varepsilon\right). & (6.31 \text{ bis}) \end{aligned} \right\}$$

Using the numerical values of  $\kappa, \lambda, M, p_0$ , already quoted, we get the curves of Fig. 7.13 where the points corresponding to total distortion of 1, 2, 3, 4, and 8 per cent are clearly marked.

In comparison, we can reason that relatively larger strains will occur at each stage of a *drained* test. In Fig. 7.14(a) we consider both drained and undrained compression tests when they have reached the same stress ratio  $\eta > 0$ . From eq. (6.14) we have

$$\frac{\dot{v}^p}{v} = \frac{\dot{v}_\kappa}{v} = (M - \eta)\dot{\epsilon} \quad (\dot{\epsilon} > 0)$$

so that in each test there will be the same shift of swelling line  $\dot{v}_\kappa$  for the same increment of distortion  $\dot{\epsilon}$ . The yield curves relevant to the successive shifts of swelling line are lightly sketched in Fig. 7.14(a). We see the undrained test slanting across them from  $U_1$  to  $U_2$  while the drained test goes more directly from  $D_1$  to  $D_2$ . It follows that for the same increment of distortion  $\dot{\epsilon}$  there will be a greater increment of  $\dot{\eta}$  in an undrained test than in a drained test, which explains the different curves of  $q/p$  versus  $\epsilon$ , in Fig. 7.14(b).

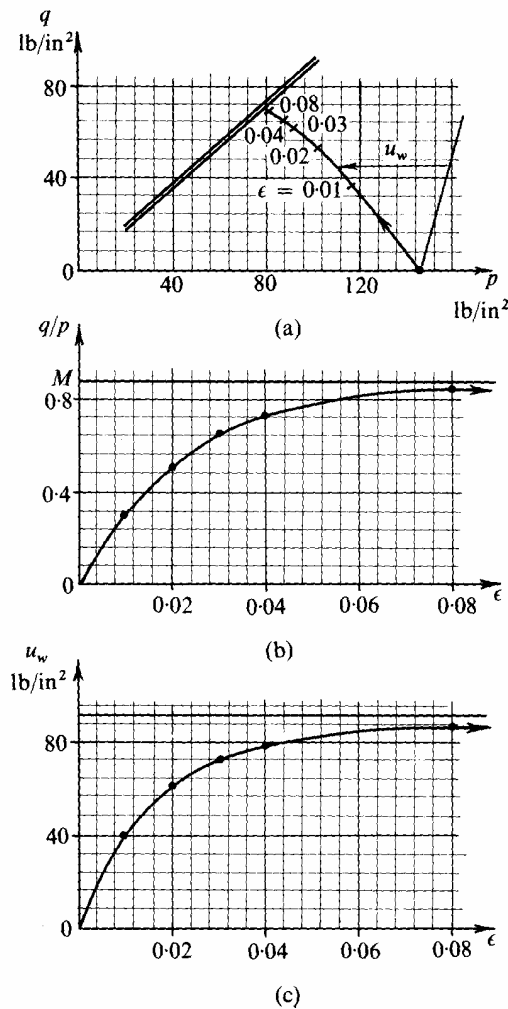


Fig. 7.13 Predicted Strain Curves for Undrained Axial Compression Test of Fig. 7.12

\* For the *undrained* test, differentiating eq. (6.27) we get  $(\lambda\dot{\eta}/M) = -\dot{p}/q$  which equals the plastic volume change  $\dot{v}_\kappa/v_0$  (since  $\dot{v} \equiv 0$ ) and hence we have eq. (7.5). For the *drained* test, differentiating eq. (6.19) we get  $\dot{\eta} = (M/\lambda - \kappa)\{\dot{v} - (\lambda\dot{p}/p)\}$  and since  $\dot{q}/\dot{p} = 3$  we also have  $\dot{\eta} = \dot{q}/\dot{p} - \lambda\dot{p}/p^2 = (3 - \eta)\dot{p}/p = (3 - \eta)(\dot{v} - \dot{v}_\kappa)$ . Eliminating  $\dot{p}$  and  $\dot{v}$  we obtain eq. (7.6).

We can, in fact, derive expressions for these quantities. It can readily be shown\* that for the increment  $U_1U_2$  in the *undrained* test

$$\frac{\kappa A}{M} \dot{\eta} = (M - \eta)v_0 \dot{\epsilon}_{\text{undrained}} \quad (v = v_0) \tag{7.5}$$

whereas for  $D_1D_2$  in the *drained* test

$$\lambda A \left( \frac{1}{M} + \frac{1}{3 - \eta} \right) \dot{\eta} = (M - \eta)v_0 \dot{\epsilon}_{\text{drained}} \tag{7.6}$$

(where  $v$  varies as the test progresses and is  $\leq v_0$ ).

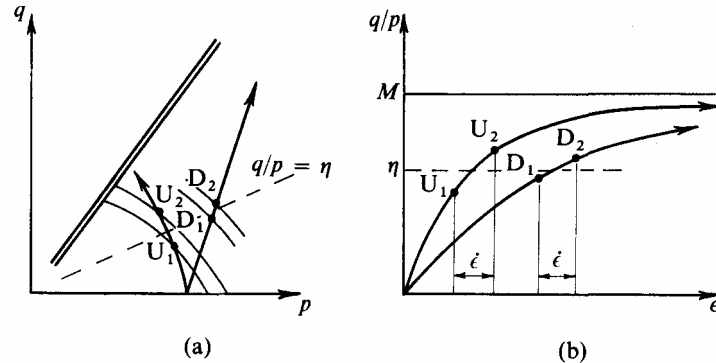


Fig. 7.14 Relative Strains in Undrained and Drained Tests

Hence the ratio of distortional strains required for the *same increment of  $\eta$*  is

$$\frac{\dot{\epsilon}_d}{\dot{\epsilon}_u} = \frac{\lambda(3 - \eta + M)v_0}{\kappa(3 - \eta)v_d} \tag{7.7}$$

and we shall expect for specimens of remoulded London clay (a) at the start of a pair of tests when

$$\left. \begin{array}{l} \eta = 0 \\ v_d = v_0 \end{array} \right\} \frac{\dot{\epsilon}_d}{\dot{\epsilon}_u} \cong 3.37$$

and (b) by the end when  $\eta \rightarrow M$  and  $v_d \cong 0.95v_0$ ,  $(\dot{\epsilon}_d/\dot{\epsilon}_u) \cong 3.52$ . It so happens that the minor influences of changing values of  $\eta$  and  $v$  during a pair of complete tests almost cancel out; and to all intents and purposes the ratio  $\dot{\epsilon}_d/\dot{\epsilon}_u$  remains effectively constant (3.45 in this case).

This constant ratio between the increments of shear strain  $\dot{\epsilon}_d/\dot{\epsilon}_u$  will mean that the cumulative strains should also be in the same ratio. This is illustrated in Fig. 7.15 where results are presented from strain controlled tests by Thurairajah<sup>9</sup> on specimens of virgin compressed kaolin. The strains required to reach the same value of the stress ratio  $\eta$  in each test are plotted against each other, giving a very flat curve which marginally increases in slope as expected.

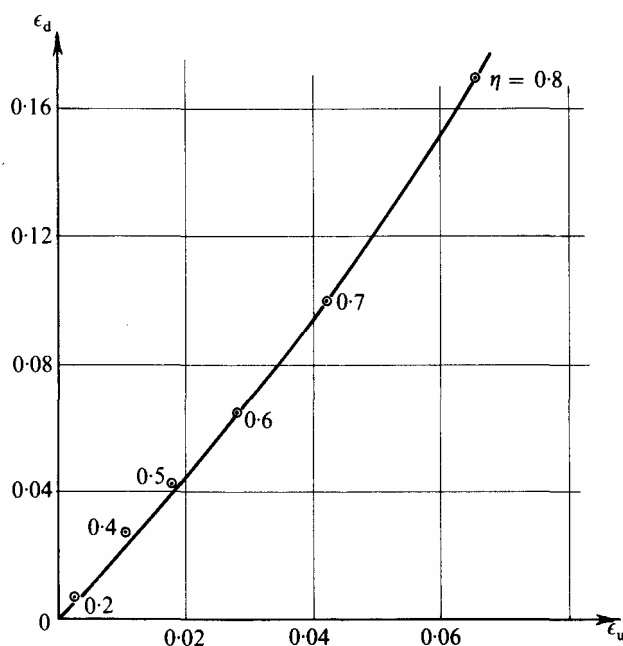


Fig. 7.15 Comparison of Shear Strains in Drained and Undrained Axial Compression Tests on Virgin Compressed Kaolin (After Thurairajah)

However, in general, plots with cumulative strain  $\epsilon$  as base are unsatisfactory for two reasons. First,  $\epsilon$  increases without limit and so each figure is unbounded in the direction of the  $\epsilon$ -axis: this contrasts strikingly with the plots in  $(p, v, q)$  space where the parameters have definite physical limits and lie in a compact and bounded region. Secondly, and of greater importance, different test paths ending at one particular state  $(p, v, q)$  will generally require different magnitudes  $\epsilon$ , so that the *total* distortion experienced by a specimen depends on its stress history and is not an absolute parameter. In contrast, the strain *increment*  $\dot{\epsilon}$  is a fundamental parameter and is uniquely related at all stages of a test on Cam-clay to the current state of the specimen  $(p, v, q)$  and the associated stress-increments  $(\dot{p}, \dot{q})$ . In effect, a soil specimen, unlike a perfectly elastic body, is unaware of the datum for  $\epsilon$  chosen by the external agency. In the following section we will consider the possibilities of working in terms of relative strain rates.

## 7.8 Interpretation of Data of $\dot{\epsilon}$ , and Derivation of Cam-clay Constants

In §7.4 we mentioned work by Parry which gave support to the critical state concept. He also plotted two sets of data as shown in Fig. 7.16 where rates of change of pore-pressure or volume change occurring at *failure* have been plotted against  $(p_u/p_f)$ . (Failure is defined as the condition of maximum deviator stress  $q$ .) This ratio is that of the critical state pressure  $p_u$ , (corresponding to the specimen's water content  $w_f$  in Fig. 7.5) to its actual effective spherical pressure at failure  $p_f$ ; this ratio is a measure of how near failure occurs to the critical state, and could just as well be measured by the difference between  $v_\lambda$  at failure and the value  $v_\lambda \cong \Gamma$  for the critical state  $\lambda$ -line.

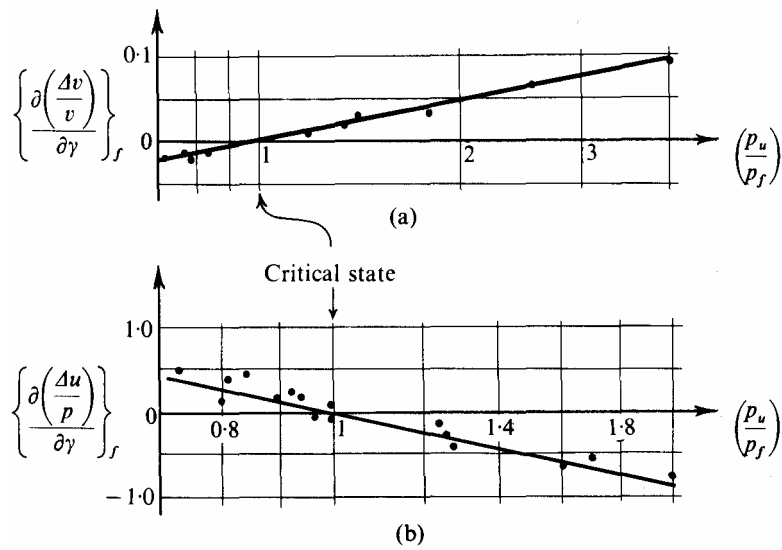


Fig. 7.16 Rates of Volume Change at Failure in Drained Tests, and Rates of Pore-pressure change at Failure in Undrained Tests on London clay (After Parry) Critical state

In the upper diagram, Fig. 7.16(a), results of drained tests are given in terms of the rate of volume change expressed by

$$\left\{ \frac{\partial \left( \frac{\Delta v}{v} \right)}{\partial \gamma} \right\}_f$$

which is equivalent to

$$-\frac{2}{300} \left( \frac{\dot{v}}{v \dot{\epsilon}} \right)_f$$

This clearly shows that the further failure occurs from the critical state the more rapidly the specimen will be changing its volume.

Conversely, in Fig. 7.16(b) the results of undrained tests are presented in terms of rate of pore-pressure change expressed by

$$\left\{ \frac{\partial \left( \frac{\Delta u}{p} \right)}{\partial \gamma} \right\}_f$$

which is equivalent to

$$+\frac{2}{300} \left( \frac{\dot{u}}{p \dot{\epsilon}} \right)_f$$

This clearly shows that the further failure occurs from the critical state the more rapidly the specimen will be experiencing change of pore-pressure.

In each case the existence of the critical state has been unequivocally established, together with the fact that the further the specimen is from this critical state condition at failure the more rapidly it is tending towards the critical state.

In the case of Cam-clay it is possible to combine these two sets of results. Our processing of data in §7.3 has provided values of  $v_\lambda$  which tell us on which  $\lambda$ -line the state



of a specimen is at any stage of a test. We also know values of  $v_\kappa$  and  $\dot{v}_\kappa/v\dot{\varepsilon}$  which represent the current  $\kappa$ -line and the rate (with respect to distortion) at which the specimen is moving across  $\kappa$ -lines. The prediction of the Cam-clay model is that for *all* compression tests (whether drained, undrained, constant- $p$ .. .) the data after yield has begun should obey eq. (6.14a)

$$\frac{\dot{v}_\kappa}{v\dot{\varepsilon}} = M - \frac{q}{p} = M - \eta \quad (7.8)$$

and while the state of the specimen is crossing the stable-state boundary surface we have from eq. (6.19)

$$\eta = \frac{M}{(\lambda - \kappa)}(\Gamma + \lambda - \kappa - v_\lambda). \quad (7.9)$$

Combining these we have

$$\frac{\dot{v}_\kappa}{v\dot{\varepsilon}} = \frac{M}{(\lambda - \kappa)}(v_\lambda - \Gamma) \quad (7.10)$$

which is a simple linear relationship between the rate of movement towards the critical state  $\dot{v}_\kappa/v\dot{\varepsilon}$  with the distance from it ( $v_\lambda - \Gamma$ ), and one which effectively expresses Parry's results of Fig. 7.16. It is possible to express the predictions for Cam-clay in terms of Parry's parameters and obtain relationships which are very nearly linear on the semi-logarithmic plots of Fig. 7.16. The relationships are for undrained tests

$$\frac{3\dot{u}}{p\dot{\varepsilon}} = \frac{\dot{v}_\kappa}{\dot{\varepsilon}} \frac{M + (3 - \eta)A}{A}$$

and for drained tests

$$\frac{\dot{v}}{v\dot{\varepsilon}} = -\frac{\dot{v}_\kappa}{v\dot{\varepsilon}} \frac{M + (3 - \eta)A}{M(1 - A)}.$$

The experimental data are such that values of  $\eta$  and  $v_\lambda$  are determined to much greater accuracy than  $\dot{v}_\kappa/v\dot{\varepsilon}$  and it is better to present them in the two separate relationships of eqs. (7.8) and (7.9) than the combined result of (7.10). The predicted results will be as in Fig. 7.17; a specimen of Cam-clay in an undrained test starting at some state such as A will remain rigid (without change of  $v_\lambda, v_\kappa$  or  $\varepsilon$ ) until B, and then yield until C is reached. Similarly, we shall have the theoretical path DEC for a specimen denser (or dryer) than critical.

We shall expect real samples to deviate from these ideal paths and are not surprised to find real data lying along the dotted paths, which cut the corners at B and particularly at E. We also know that we have taken no account of the small permanent distortions that really occur between A and B or between D and E, and some large scatter is to be expected in the calculation of  $\dot{v}_\kappa/v\dot{\varepsilon}$  when  $\dot{\varepsilon}$  is small. However, the plot of Fig. 7.17 will allow us to make a reasonable estimate of a value of  $M$  which we may otherwise find difficult. A direct assessment from the final value of  $q/p$  of Fig. 7.14(b) could only be approximate on account of the inaccuracies in measurement of the stress parameters at large strain, and would underestimate  $M$  because failure intervenes before the critical state is reached.

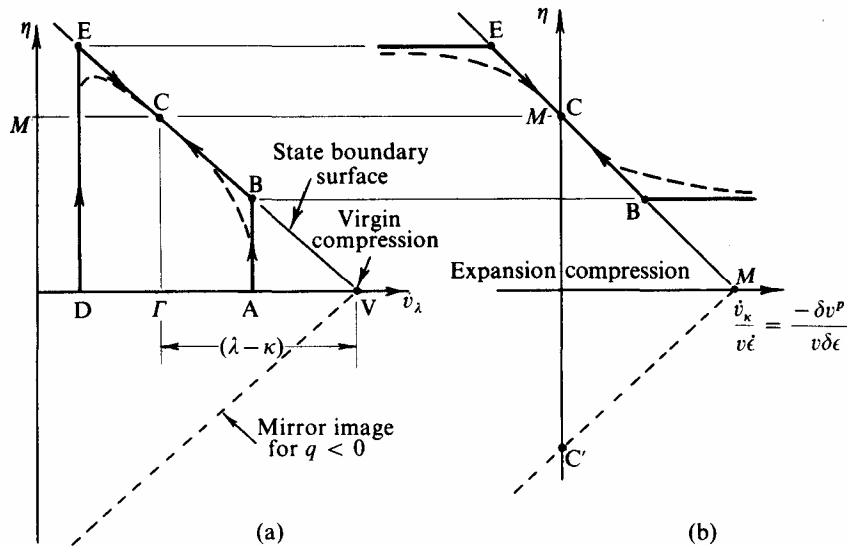


Fig. 7.17 Predicted Test Results for Axial Compression Tests on Cam-clay

Results of a very slow strain-controlled undrained test on kaolin by Loudon are presented in Figs. 7.18 and 7.19 and are tabulated in appendix B. This specimen was initially under virgin compression, but experimentally we can not expect that the stress is an absolutely uniform effective spherical pressure. Any variation of stress through the interior of the specimen must result in mean conditions that give a point A not quite at the very corner V. These initial stress problems are soon suppressed and over the middle range of the test the data in Fig. 7.18 lie on a well defined straight line which should be of slope  $(M)/(\lambda - \kappa)$ . As we have already established values for  $\kappa$  and  $\lambda$ , we can use them to deduce the value of  $M$ . For the quoted case of kaolin  $\lambda = 0.26, \kappa = 0.05$  and so  $M \cong 1.02$  and  $\Gamma \cong 3.265$ .

For a series of similar tests we shall expect some scatter (even in specially prepared laboratory samples) and it will be necessary to take mean values for  $M$  and  $\Gamma$ . It should be noted that failure as defined by the condition of maximum deviator stress  $q$ , occurs well before the condition of maximum stress ratio  $\eta$ , is reached.

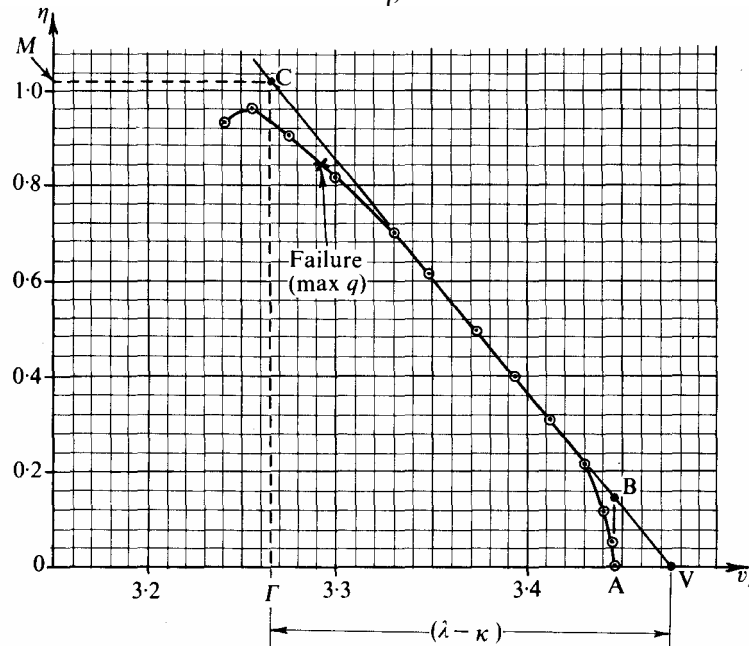


Fig. 7.18 Test Path for Undrained Axial Compression Test on Virgin Compressed Kaolin (After Loudon)

Turning to Fig. 7.19, the results indicate the general pattern of Fig. 7.17(b) but in detail they show some departure from the behaviour predicted by the Cam-clay model. The intercepts of the straight line BC should be  $M$  on both axes; but along the abscissa axis the scale is directly proportional to  $\kappa$  so that any uncertainty in measurement of its value will directly affect the position of the intercept.

Thus, in order to establish Cam-clay constants for our interpretation of real axial-test data we need two plots as follows:

(a) Results of isotropic consolidation and swelling to give  $v$  against  $\ln p$  as Fig. 7.3 and hence values for  $\kappa$  and  $\lambda$ .

(b) Results of conventional undrained compression test on a virgin compressed specimen to give  $v_z$  against  $\eta$  as Fig. 7.18 and hence values of  $M$  and  $\Gamma$ .

Having established reasonable mean values for these four constants we can draw the critical state curve, the virgin compression curve, and the form of the stable-state boundary surface, and in Fig. 7.20 we can use these predicted curves as a fundamental background for interpretation of the real data of subsequent tests.

At this stage we must emphasize that the interpretation is concerned with stress-strain relationships, and *not* with failure which we will discuss in chapter 8. We also note that there are *two* alternative ways of estimating the critical state and Cam-clay constants. The data of ultimate states in *slow* tests, in sufficient quantity, will define a critical state line such as is shown in Fig. 7.5. The slow tests cannot be used for close interpretation of their early stages when the data look like Fig. 7.21 and indicate a specimen that is not in equilibrium. However, from the data of slow axial tests and of the semi-empirical index tests, we can obtain a reasonable estimate of the critical state and Cam-clay constants. The second alternative is to use a few *very slow* tests and subject the data to a close interpretation. Although in Fig. 7.20 we concentrate attention on undrained tests, the interpretive technique is equally appropriate to very slow drained tests.

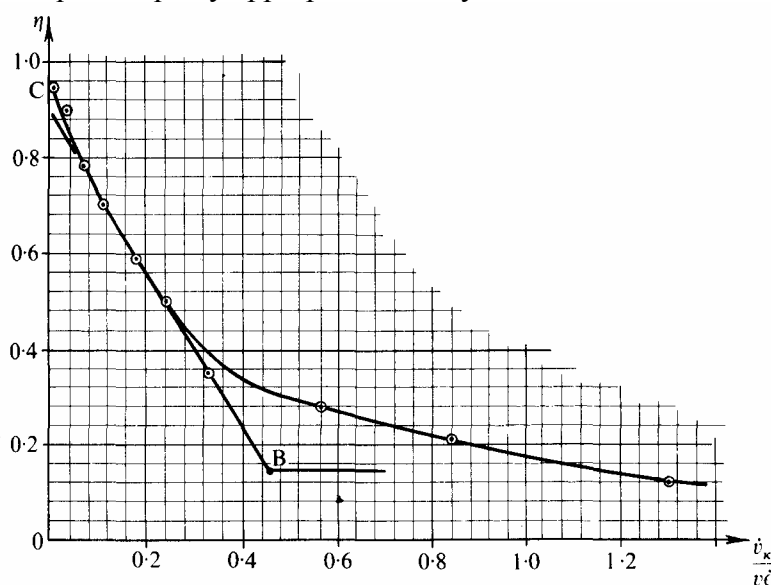


Fig. 7.19 Rate of Change of  $v$  during Undrained Axial Compression Test on Virgin Compressed Kaolin (After Loudon)

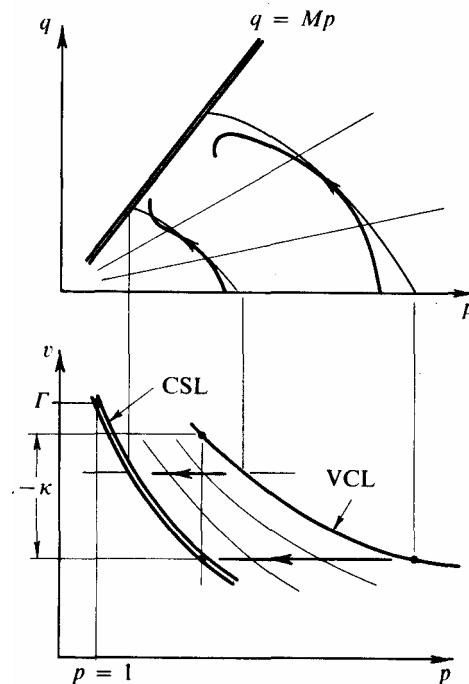


Fig. 7.20 Cam-clay Skeleton for Interpretation of Data

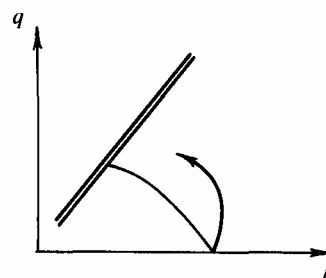


Fig. 7.21 Test Path for Test Carried out too quickly

## 7.9 Rendulic's Generalized Principle of Effective Stress

Experiments of the sort that we outlined in §7.1 were performed by Rendulic in Vienna and reported<sup>10</sup> by him in 1936. He presented his data in principal stress space, in the following manner. First he analysed the data of *drained* tests and plotted on the  $(\sigma'_1, \sqrt{(2)}\sigma'_3)$  plane contours of constant water content; that is to say, if at  $\sigma'_1 = 125 \text{ lb/in}^2$  and  $\sigma'_3 = 115 \text{ lb/in}^2$  in one test that specimen has the same water content as another specimen at  $\sigma'_1 = 128 \text{ lb/in}^2$  and  $\sigma'_3 = 108 \text{ lb/in}^2$  in a different test then the points (125, 115) and (128, 108) would lie on one contour. Rendulic plotted the data of effective stress in *undrained* tests and found that these data lay along one or other of his previously determined contours. He thus made a major contribution to the subject by establishing the generalized principle of effective stress; for a given clay in equilibrium under given effective stresses at given initial specific volume, the specific volume after any principal stress increments was uniquely determined by those increments. This principle we embody in the concept of one stable-state boundary surface and many curved 'elastic' leaves as illustrated in Fig. 6.5: a small change  $(\dot{p}, \dot{q})$  will carry the specimen through a well defined change  $\dot{v}$  which may be partly or wholly recoverable. We could have mentioned the

contours of constant specific volume at an earlier stage but we have kept back our discussion of Rendulic's work until this late stage in order that no confusion can arise between our yield curves and his constant water content contours.

Rendulic<sup>11</sup> emphasized the importance of stress – strain theories rather than failure theories. He found that the early stages of tests gave contours that were symmetrical about the space diagonal, while states at failure lay unsymmetrically to either side. This led him to consider that *yielding* was governed by a modification of Mises' criterion with yield surfaces of revolution about the space diagonal, while *failure* might be governed by a different criterion.

In Henkel's slow strain-controlled axial tests on saturated remoulded clay that we have already quoted so extensively, the tests were timed so that there were virtually no pore-pressure gradients left at *failure*. Before failure, in the early stages of tests, these data do not define effective stress states with the same accuracy that lies behind Fig. 7.12. A precise comparison of Figs. 7.12 and 7.23 will quickly reveal differences between the two. However, the general concept and execution of these tests makes them worth close study. His interpretation<sup>12</sup> follows Rendulic's approach. In Fig. 7.22 he plots contours from drained tests and stress paths for undrained tests of a set of specimens all initially *virgin compressed*. In Fig. 7.23 he plots, in the same manner, data of a set of specimens all initially *overcompressed* to the same pressure 120 lb/in<sup>2</sup> and allowed to swell back to different pressures. These contours correspond respectively to our stable-state boundary surface (with some differences associated with early data of slow tests) and to the elastic wall that was discussed for Cam-clay. Cam-clay is only a conceptual model and clearly Figs. 7.22 and 7.23 show significant deviation for isotropic behaviour from the predictions of the simple model. The Figs. 7.22 and 7.23 also show data of failure which will be discussed in detail later.

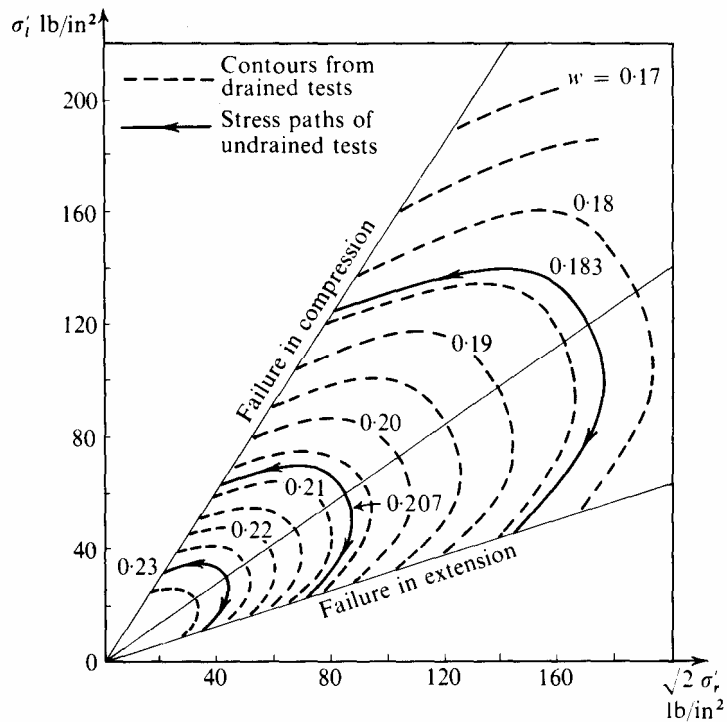


Fig. 7.22 Water Content Contours from Drained Tests and Stress Paths in Undrained Test for Virgin Compressed Specimens of Weald Clay (After Henkel)

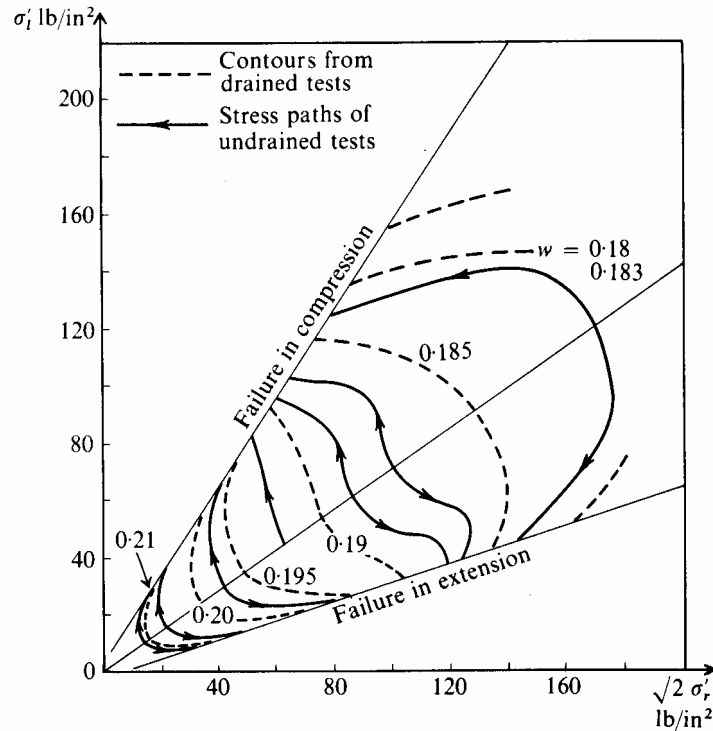


Fig. 7.23 Water Content Contours from Drained Tests and Undrained Stress Paths for Specimens of Weald Clay having a Common Consolidation Pressure of 120 lb/in<sup>2</sup> (After Henkel)

Rendulic clearly explained the manner in which pore-pressure is generated in saturated soil, and separated the part of the total stress that could be carried by the effective soil structure from the part of the total stress that had to be carried by pore-pressure. In the light of our development of the Cam-clay model, we can restate the generalized effective stress principle in an equivalent form: 'If a soil specimen of given initial specific volume, initial shape, and in equilibrium under initial principal effective stresses is subject to any principal strain-increments then these increments uniquely determine the principal effective stress-increments'.

The generalized principle of effective stress in one form or another makes possible an interpretation of the change of pore-pressure.

## 7.10 Interpretation of Pore-pressure Changes

Change of *effective* stress in soil depends on the deformation experienced by the effective soil structure. The pore-pressure changes in such a manner that the *total* stress continues to satisfy equilibrium.

Attempts have been made to relate such change of pore-pressure to change of total stress. Curves such as those in Fig. 7.13(c) have been observed in studies of axial tests on certain soft clays where the increase in major principal total stress was matched by the rise in pore-pressure. For example, if a virgin compressed specimen under initial total stresses

$$\sigma_r = 80 \text{ lb/in}^2 \quad \sigma_l = 80 \text{ lb/in}^2 \quad u_w = 50 \text{ lb/in}^2$$

was subjected to a total stress-increment  $\dot{\sigma}_l = 10 \text{ lb/in}^2$ , it would come into a final equilibrium with

$$\sigma_r = 80 \text{ lb/in}^2 \quad \sigma_l = 90 \text{ lb/in}^2 \quad u_w = 60 \text{ lb/in}^2$$

The simple hypothesis which was first put forward was that the ratio of pore-pressure increment  $\dot{u}_w$  to major principal total stress-increment  $\dot{\sigma}_l$  was simply

$$\frac{\dot{u}_w}{\dot{\sigma}_l} = 1. \quad (7.11)$$

This relationship was modified by Skempton<sup>13</sup> who proposed the use of pore-pressure parameters  $A$  and  $B$  in a relationship

$$\dot{u}_w = B\{\dot{\sigma}_r + A|\dot{\sigma}_l - \dot{\sigma}_r|\} \quad (7.12)$$

Here,  $B$  is a measure of the saturation of the specimen; for full saturation  $B=1$ . The parameter  $A$  multiplies the effect of  $q$  and relates the curves (b) and (c) of Fig. 7.13. An alternative coefficient introduced by Skempton for the case  $\dot{\sigma}_l > \dot{\sigma}_r$  is

$$\frac{\dot{u}_w}{\dot{\sigma}_l} = \bar{B} = B\left\{1 - (1 - A)\left(1 - \frac{\dot{\sigma}_r}{\dot{\sigma}_l}\right)\right\}. \quad (7.13)$$

In either form, if we introduce full saturation ( $B=1$ ), and consider only the *compression* test ( $\dot{\sigma}_r = 0$ ), both eqs. (7.12) and (7.13) reduce to

$$A = \frac{\dot{u}_w}{\dot{q}} \quad \bar{B} = \frac{\dot{u}_w}{\dot{\sigma}_l} - \frac{\dot{u}_w}{\dot{q}}. \quad (7.14)$$

The simple hypothesis eq. (7.11) suggested that for virgin compressed clay a basis for prediction of pore-pressures would be  $A = \bar{B} = 1$ .

In Fig. 7.24(a) we show the predicted undrained test path for a virgin compressed Cam-clay specimen. The point V is an initial state, point W represents applied *total* stress and point X represents applied *effective* stress. For the simple case, when  $\sigma_r = \text{const.}$  and  $\dot{\sigma}_r = 0$  which we show in the figure,

$$\dot{u}_w + \dot{p} = \frac{\dot{q}}{3}.$$

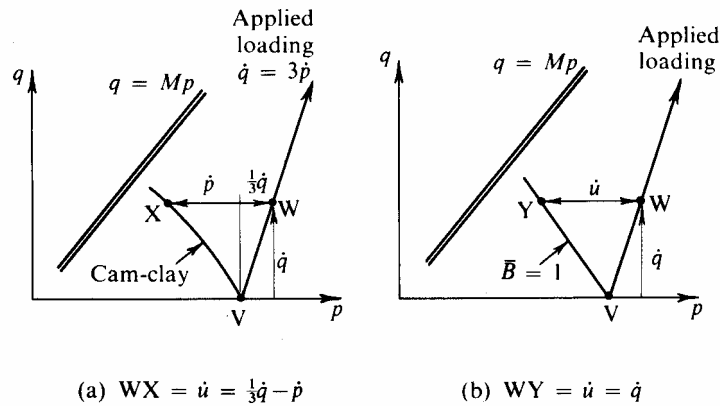


Fig. 7.24 Comparison of Cam-clay with  $\bar{B} = 1$  Hypothesis

The yielding of Cam-clay in an undrained test was discussed in §6.7, where eq. (6.27) determines the changing *effective* stresses ( $q, p$ ), and defined the Cam-clay path of Fig. 7.24(a) which is close to a straight line. In Fig. 7.24(b) we show the changing effective stresses that would be applicable to a material for which  $\bar{B} = 1$ . The  $\bar{B} = 1$  hypothesis is only a little different from the prediction of Cam-clay, for which it can be shown that

$$\bar{B} = \frac{\dot{u}_w}{\dot{q}} = \frac{1}{3} - \frac{\dot{p}}{\dot{q}} = \frac{1}{3} + \frac{A}{M - A\eta} \quad (7.15)$$

for this type of test.

We will next consider what we have called ‘over compressed’ specimens, meaning specimens that have been virgin compressed under a high effective spherical pressure  $Np_0$

and then permitted to swell back under a reduced effective spherical pressure  $p_0$ . In Fig. 7.25 on the graph  $v$  versus  $\ln p$  we see the sequence of virgin compression to  $Np_0$  at point J, followed by swelling to an effective pressure  $p_0$  and a specific volume  $v_0$  at point K. Points I and L are on the virgin compression and critical state lines at specific volume  $v_0$ . Swelling from J to K, with reduction of effective spherical pressure from  $Np_0$  to  $p_0$ , results in increase of specific volume of  $(\kappa \ln N)$ . So we can calculate that the effective spherical pressures at I and L are

$$\left. \begin{aligned} \ln p_e &= \ln Np_0 - \frac{\kappa}{\lambda} \ln N, \\ \ln p_u &= \ln p_e - A \\ \therefore \text{for K, } \ln\left(\frac{p_0}{p_u}\right) &= A(1 - \ln N), \end{aligned} \right\} \quad (7.16)$$

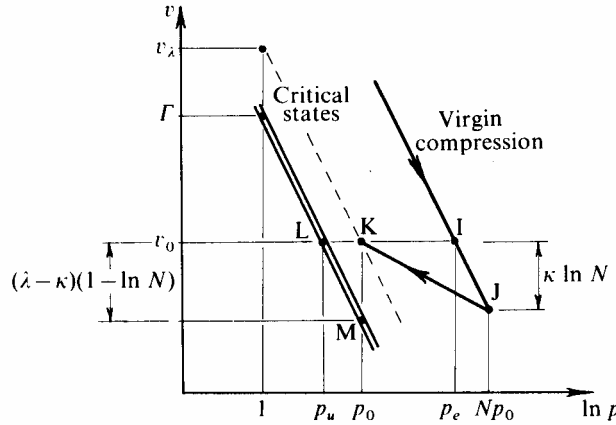


Fig. 7.25 Increase of Specific Volume during Isotropic Swelling in terms of Overcompression Ratio

and the separation of K from the critical state line is

$$KM = \lambda \ln\left(\frac{p_0}{p_u}\right) = (\lambda - \kappa)(1 - \ln N). \quad (7.17)$$

We have already defined the offset  $KM$  as  $(v_\lambda - \Gamma)$ , so that for any general point

$$v_\lambda - \Gamma = (\lambda - \kappa)(1 - \ln N) \quad (7.18)$$

from which we see at once that a family of specimens all having the same overcompression ratio  $N$  will have the same value of  $v_\lambda$ , i.e., lie on the same  $\lambda$ -line.

We can see in Fig. 7.26 the manner in which the pore-pressure  $u_w$  develops in an undrained compression test on an initially overcompressed specimen. The line KQ represents the applied total loading; and the curve KRL represents the behaviour of Cam-clay consisting of an initial elastic part KR and subsequent plastic part RL of the state path approaching the critical state at L. The ultimate pore-pressure  $u_u$  if the critical state  $(p_u, q_u = Mp_u)$  were reached would be

$$u_u = p_0 - p_u + \frac{1}{3}Mp_u.$$



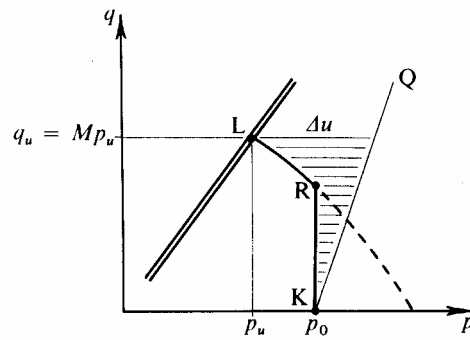


Fig. 7.26 Development of Pore-pressure during Undrained Compression Test on Overcompressed Specimen

Let us introduce a parameter  $A_u$  defined by

$$A_u = \frac{u_u}{q_u} = \frac{u_u}{Mp_u} \tag{7.19}$$

so that

$$A_u = \frac{p_0 - p_u + \frac{1}{3}Mp_u}{Mp_u}$$

But from eq. (7.17)

$$\frac{p_0}{p_u} = \exp\{\lambda(1 - \ln N)\} = (\exp \lambda)N^{-\lambda}$$

$$\therefore MA_u = (\exp \lambda)N^{-\lambda} - 1 + \frac{1}{3}M \tag{7.20}$$

For the case of London clay with  $\lambda = 0.614$  and  $M = 0.888$  this becomes

$$A_u \cong 2N^{-0.614} - 0.8. \tag{7.21}$$

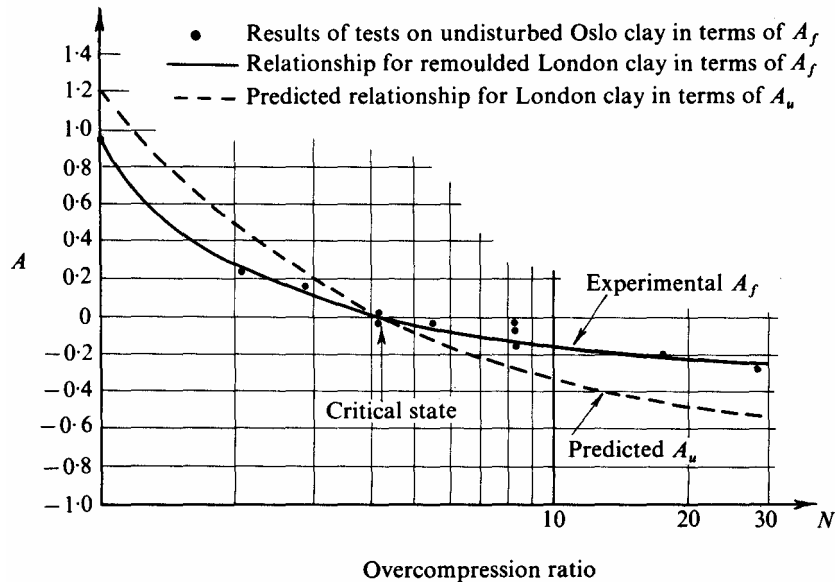


Fig. 7.27 Relationship between Pore-pressure Parameter  $A$  and Over-compression Ratio  $N$  (After Simons)

In Fig. 7.27 we show data of pore-pressure coefficient  $A_f$  observed at *failure* on sets of overcompressed specimens of undisturbed Oslo clay and remoulded London clay quoted

by Simons<sup>14</sup>. For comparison, the dotted line is the relationship predicted by eq. (7.21) for London clay for the pore-pressure coefficient  $A_u$  appropriate to the *critical state*.

From the work by Parry already quoted, we shall expect that on the wet (or loose) side of the critical state line  $A_f < A_u$  and on the dry (or dense) side  $A_f > A_u$ . The cross-over of the experimental and predicted curves must occur when  $A_f = A_u = 0$ , which from eq. (7.21) will be when

$$N = 2.5^{1/0.614} = 4.45.$$

This pattern of behaviour is borne out in Fig. 7.27 and the fact that it is the same for the remoulded London clay specimens as for the undisturbed Oslo clay specimens suggests that the critical state concept has wide application.

However, we must emphasize that the pore-pressure parameter  $A$  is not itself a fundamental soil property. In Fig. 7.28(b) we illustrate the overcompression of two specimens  $X$  and  $Y$  and the virgin compression of a specimen  $W$ . In Fig. 7.28(a) we illustrate the changing effective stresses that would occur in undrained tests on these three specimens. At failure each has approached the near vicinity of the critical state  $C$ . *En route* to failure, the pore-pressure  $u_w$  is the horizontal offset between the faint lines  $WW'$ ,  $XX'$ ,  $YY'$  that represent total stress application and the firm lines  $WC$ ,  $XC$ ,  $YC$  that represent effective stress response. For specimen  $W$  the simple hypothesis  $\bar{B} = 1$  has some meaning, but not for specimen  $Y$  where the pore-pressures show small initial positive values followed by subsequent negative pore-suction.

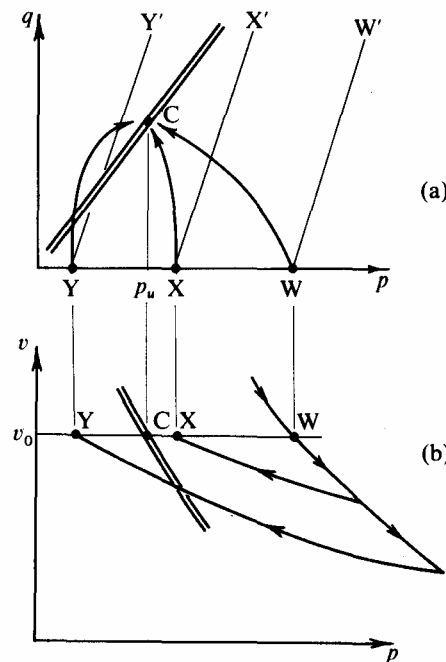


Fig. 7.28 Differing Pore-pressure Responses of Specimens with differing Amounts of Overcompression

There is nothing fundamentally significant about the applied loading lines. Other loading conditions would give different inclinations to these lines. The strains of the deforming effective soil structure, as it yields and approaches  $C$  from  $W$  or  $X$  or  $Y$ , do bear a fundamental relationship to the *effective* stresses. The pore-pressure simply carries whatever excess there may be of total pressure over and above effective spherical pressure.

We can take an example, other than the axial-test situation, and consider the advance of a pile tip in a layer of clay initially in a state of virgin plastic compression.

Figure 7.29(a) shows two positions I and II in the advance of that pile, and a small elemental specimen of clay being displaced. The geometry of displacement imposes on the specimen some increment of distortion  $\dot{\epsilon}$ , see Fig. 7.29(b), and the rapid advance of the pile ensures that there is no drainage or volume change of the specimen. If the initial state  $(q, p)$  of the specimen is point I in Fig. 7.29(c), the subsequent state II is completely determined by the distortion  $\dot{\epsilon}$  at constant volume. As the pile tip advances, the deforming clay must experience a *fall* in effective pressure. The clay specimen moves relatively closer to the pile tip and total pressure must *rise* during the increment. There will be a marked rise in pore-pressure to ensure that total stresses continue to be in equilibrium round the pile tip. In general it seems that the analysis of such problems does not involve the pore-pressure parameters, but does require some fundamental statements of a relationship between change of effective stress and the deformation experienced by the effectively stressed soil.

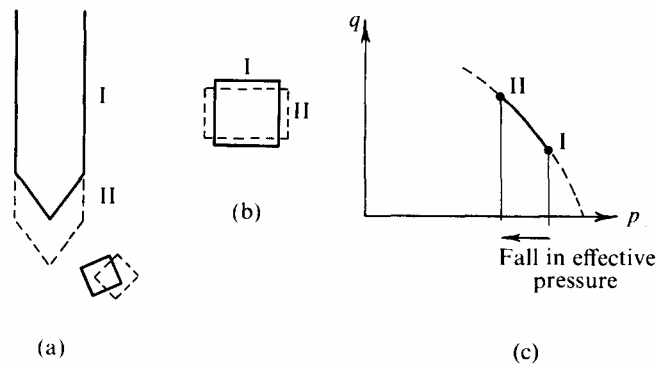


Fig. 7.29 Pressure Change caused by Advance of Tip of Pile

## 7.11 Summary

The close interpretation of data of very slow strain-controlled axial tests on saturated clay specimens has proved most rewarding. The position has been described in detail because it is hoped that it will prove to be of value to engineers who are involved in soil testing. In §7.8 we introduced new methods of plotting data which are illustrated in Figs. 7.18 and 7.19, and at the end of §7.8 it is concluded that the combination of Figs. 7.3 and 7.18 will give the best basis for interpretation of test data.

The last two sections, §7.9 and §7.10, have reviewed two notable alternative interpretations of the data of axial testing. The plotting of contours of constant water content by Rendulic produces an interesting display of data, and after our detailed development of the Cam-clay model we can appreciate the great contribution that was made by Rendulic's work. The introduction of pore-pressure parameters  $A$ ,  $B$ , and  $\bar{B}$  is particularly interesting in showing how  $\bar{B} = 1$  corresponds well with the Cam-clay model. However, neither Rendulic's approach nor the use of pore-pressure parameters seem to offer us as complete an interpretation as can be obtained by introduction of the critical state and Cam-clay models.

When the new soil constants are obtained by interpretation of test data the question that immediately arises is of their *use* in design calculation. It is evident that the Coulomb failure criterion which we will approach in the next chapter is the main model with which design calculations are presently made. However, it will prove possible to use our new understanding of the yielding of soil to make a rational choice of Coulomb strength parameters for design calculations: in this sense the new constants may prove to be useful.

*References to Chapter 7*

- <sup>1</sup> Bishop, A. W. and Henkel, D. J. *The Measurement of Soil Properties in the Triaxial Test*, Arnold, 1957.
- <sup>2</sup> Andresen, A. and Simons, N. E. Norwegian Triaxial Equipment and Technique, *Proc. Res. Conf on Shear Strength of Cohesive Soils*, A.S.C.E., Boulder, pp. 695—709, 1960.
- <sup>3</sup> Schofield, A. N. and Mitchell, R. 3. Correspondence on “‘Ice Plug” Stops in Pore Water Leads”, *Geotechnique* 17, 72 – 76, 1967.
- <sup>4</sup> Rowe, P. W. and Barden. L. Importance of Free Ends in Triaxial Testing, *Journ. Soil Mech. and Found. Div.*, A.S.C.E., 90, 1 – 27, 1964.
- <sup>5</sup> Loudon, P. A. *Some Deformation Characteristics of Kaolin*, Ph.D. Thesis, Cambridge University, 1967.
- <sup>6</sup> Henkel, D. J. The Effect of Overconsolidation on the Behaviour of Clays During Shear, *Géotechnique* 6, 139 – 150, 1956.
- <sup>7</sup> Parry, R. H. G. Correspondence on ‘On the Yielding of Soils’, *Géotechnique* 8, 184 – 6, 1958.
- <sup>8</sup> Bishop, A. W., Webb, D. L. and Lewin, P. I. Undisturbed Samples of London Clay from the Ashford Common Shaft: Strength Effective Stress Relationships, *Géotechnique* 15, 1 – 31, 1965.
- <sup>9</sup> Thuraiajah, A. *Some Shear Properties of Kaolin and of Sand*, Ph. D. Thesis, Cambridge University, 1961.
- <sup>10</sup> Rendulic, L. Pore-Index and Pore-water Pressure, *Bauingenieur* 17, 559, 1936.
- <sup>11</sup> Rendulic, L. A Consideration of the Question of Plastic Limiting States, *Bauingenieur* 19, 159 – 164, 1938.
- <sup>12</sup> Henkel, D. J. The Relationships between the Effective Stresses and Water Content in Saturated Clays, *Geotechnique* 10, 41 – 54, 1960.
- <sup>13</sup> Skempton, A. W. Correspondence on ‘The Pore-pressure Coefficient in Saturated Soils’, *Géotechnique* 10, 186 – 7, 1960.
- <sup>14</sup> Simons, N. E. The Effect of Overconsolidation on the Shear Strength Characteristics of an Undisturbed Oslo Clay, *Proc. Res. Conf on Shear Strength of Cohesive Soils*, A.S.C.E., Boulder, pp 747 – 763, 1960.